THEORETICAL PERFORMANCE OF HYDROGEN-BROMINE RECHARGEABLE SPE FUEL CELL*

R.F. Savinell and S.D. Fritts
Case Western Reserve University
Cleveland, Ohio 44106

A mathematical model was formulated to describe the performance of a hydrogen-bromine fuel cell. Porous electrode theory was applied to the carbon felt flow-by electrode and was coupled to theory describing the SPE system. Parametric studies using the numerical solution to this model have been performed to determine the effect of kinetic, mass transfer, and design parameters on the performance of the fuel cell. The results indicate that the cell performance is most sensitive to the transport properties of the SPE membrane. The model was also shown to be a useful tool for scale-up studies.

INTRODUCTION

Hydrogen-bromine fuel cells are of interest as both primary and regenerative energy storage systems. The fuel cell system can be coupled with solar cell arrays to provide the power necessary to charge the system. The regenerative capability of hydrogen-bromine fuel cell systems, along with their high energy densities, make them excellent candidates for space power applications.

The electrochemical reactions for the hydrogen-bromine system are nearly reversible, and the use of solid polymer electrolytes has eliminated cell gaps. Consequently, good energy storage efficiencies can be obtained even at high current density operation.

High current density operation requires reactor designs which enhance mass transfer rates. A flow system is used to improve mass transfer and to aid in thermal management.

A promising design for a hydrogen-bromine device is one having a negative half-cell with only a gas phase which is separated by a solid polymer ionic conducting membrane from a positive half-cell with a flowing aqueous electrolyte. The hydrogen and bromine are stored external to the cell, the hydrogen in the form of a metal hydride. This configuration warrants theoretical treatment for further development and scale-up. Therefore, this work has focused on the development of a theoretical model capable of predicting overall cell performance.

In this paper, a theoretical model of a hydrogen-bromine fuel cell is described. The model equations were solved by numerical techniques. The parametric studies with this model elucidate the effects of catalyst activity, mass and ion transport, and cell scale-up on single cell performance. A discussion is presented on the results of these studies.

*This Research was supported by NASA Contract NAG 3-500 and NSF award CPE-8351849

SYMBOLS

A_t = characteristic area of an SPE consisting of exposed and unexposed membrane, cm^2

a = specific electrode area (i.e. the active area per unit electrode volume), cm^{-1}

$a'^{\delta}_{Br_2}$ = surface bromine activity

$a^{f\,\delta}_{Br_2}$ = bromine activity of reactor feed

C^{δ}_{Br-} = local bulk bromide concentration, mol/l

C'^{δ}_{Br-} = surface bromide concentration, mol/l

C^{β}_{H+} = bulk β-phase concentration of protons in equilibrium with the δ-phase, mol/l

C'^{β}_{H+} = proton concentration in the β-phase at the electrode surface, mol/l

$C^{f\delta}_{Br-}$ = cell feed concentration of bromic acid, mol/l

D^{δ}_{Br} = diffusion coefficient of bromide ion in solution, mol/l

D^{β}_{H+} = effective proton diffusion coefficient in the membrane, mol/l

F = Faraday's constant, 96, 487 A-s/equil

f = fraction of SPE not in contact with the current collector

k_m = mass transfer coefficient, cm/sec

I = total current from a characteristics area (A_t), A

i = current density in the porous electrode based on the true electrode area, A/cm^2

$i_{o,ref}$ = bromine reaction exchange current density evaluated for a bromine reference electrode at cell inlet concentrations, A/cm^2

i' = hydrogen side current density, (based on membrane area) A/cm^2

$i'_{o,ref}$ = exchange current density (based on membrane area) evaluated at unit proton activity and hydrogen pressure, A/cm^2

L, L' = length and width of SPE section not in contact with current collector, cm

n = number of electrons transferred in reaction, equiv/mol

$p_{H_2}^{\alpha}$ = hydrogen partial pressure, atm.

R_s = effective membrane area resistivity, ohm-cm^2

t = porous electrode thickness, cm.

t_β = membrane thickness, cm.

t_+ = transport number for protons in the membrane

U = equilibrium cell potential, volts

v_y = plug flow solution velocity through the porous electrode, cm/sec

α_a, α_c = anodic and cathodic transfer coefficients, respectively, and usually reported as both being 1/2

δ_e = thickness of platinum catalyst layer on SPE, cm

ϵ = void fraction of bromine electrode

ϵ' = volume fraction of membrane material between platinum catalyst particles

κ = effective electrolyte conductivity, mho/cm

ρ_e = effective resistivity of platinum catalyst, ρ_e^o of solid platinum, ohm-cm

ϕ_1, ϕ_2 = bromine side metal and solution phase quasielectrostatic potentials versus a bromine reference electrode at feed concentrations, V

ϕ_1', ϕ_2' = hydrogen half cell quasielectrostatic potentials relative to a normal hydrogen electrode of the metal phase and the β-phase respectively, V

THEORY

The description of a single hydrogen-bromine cell is shown in figure 1. The hydrogen electrode is treated as a planar electrode having a current carrying bus network. The bromine electrode is a porous carbon felt.

The planar hydrogen electrode, (α-phase), is in direct contact with the solid polymer electrolyte denoted as the β-phase. The kinetic expression for the hydrogen reaction can be written according to the nomenclature and analysis of Trainham and Newman [ref. 1] as

$$i' = i'_{o,ref}\left[\left[\frac{p^{\alpha}_{H_2}}{1\ atm}\right]^{1/2} \exp\left\{\frac{\alpha_a F}{RT}(\phi'_1-\phi'_2)\right\} - \frac{C'^{\beta}_{H+}}{1\ mol/l} \exp\left\{\frac{-\alpha_c F}{RT}(\phi'_1-\phi'_2)\right\}\right] \quad (1)$$

where the nomenclature is presented above.

The partial pressure of hydrogen at the catalyst surface is assumed to be equal to that of the bulk. The kinetic expression also requires specification of the concentration of the protons at the surface of the platinum particles. The Nafion membrane is believed to be composed of clusters of hydrophilic sites in a hydrophobic matrix [ref. 2]. Protons are associated with the fixed functional sulfonate groups and with the free water phase. For our model we assumed that the protons involved with the surface reaction come from the free acid phase. Protons are then transported across the membrane through a diffusion/migration mechanism. The interfacial mass transfer can be expressed as:

$$i' = \frac{-nFD^{\beta}_{H+}}{(1-t_+)t_{\beta}} [C^{\beta}_{H+} - C'^{\beta}_{H+}] \times 10^{-3} \quad (2)$$

The concentration of protons in the membrane at the side opposite the hydrogen electrode is assumed to be in equilibrium with the adjacent HBr solution. This concentration was estimated by using a curve fit of the data given by Yeo and Chin [ref. 3], which is expressed as:

$$C^{\beta}_{H+} = -0.458 + 0.80067C^{\delta}_{Br-} + 0.023843C^{\delta\ 2}_{Br-} \quad (3)$$

We have recently begun work to examine the role of the protons associated with the fixed ions on the kinetics and to examine the proton diffusion mechanisms in Nafion membranes.

The metal phase potential, ϕ'_2, is taken to be uniform. A conductive bipolar plate feeds the current to the platinum catalyst. Although current must flow through a thin platinum layer to the bipolar plate contact point, the potential drop is estimated to be small. A simple model which justifies this assumption is described in the Appendix.

The bromine electrode performance is described by macroscopic homogeneous porous electrode theory [ref. 4,5]. The necessary descriptive equations are now summarized. The charge balance, can be written as

$$\frac{d^2\phi_2}{dx^2} = -\frac{ai}{\kappa} \quad (4)$$

with boundary conditions

$$x = 0, \quad \frac{d\phi_2}{dx} = 0 \tag{5}$$

$$x = t, \quad \phi_2 = \phi_2' + U - i'R_s \tag{6}$$

where R_s is the membrane resistivity. After neglecting diffusion in the axial direction, the conservation of mass of the bromide ion is written as

$$v_y \frac{\partial C^{\delta}_{Br-}}{\partial y} = \epsilon D^{\delta}_{Br-} \frac{\partial^2 C_{Br-}}{\partial x^2} - \frac{ai}{nF} \times 10^3 \tag{7}$$

with boundary conditions of

$$x = 0, \ t \quad \frac{dC^{\delta}_{Br-}}{dx} = 0 \tag{8}$$

$$y = 0, \quad C^{\delta}_{Br-} = C^{f\ \delta}_{Br-} \tag{9}$$

The surface concentration is related to the bulk concentration through the mass transfer coefficient, k_m, by the following expression.

$$i = nFk_m \left[C^{\delta}_{Br-} - C'^{\delta}_{Br-}\right] \times 10^{-3} \tag{10}$$

The kinetics of this reaction can be expressed by

$$i = i_{o.ref}\left[\frac{C'^{\delta}_{Br-}}{C^{f\ \delta}_{Br-}} \exp\left\{\frac{\alpha_a F}{RT}(\phi_1-\phi_2)\right\} - \left[\frac{a'^{\delta}_{Br_2}}{a^{f}_{Br_2}}\right]^{1/2} \exp\left\{\frac{-\alpha_c F}{RT}(\phi_1-\phi_2)\right\}\right] \tag{11}$$

In these calculations, the ratio of the bromine activities is taken to be unity and the carbon phase potential, ϕ_1, is assumed to be uniform.

At the membrane-porous electrode interface, the membrane current density, i', is related to the porous electrode current density, i, by the following expression:

$$\kappa \frac{d\phi_2}{dx}\bigg|_{x=t} = i' = -a \int_0^t i \, dx \tag{12}$$

The equations of this model were combined, made dimensionless, linearized, and then solved using an implicit numerical technique. The dimensionless equations are listed in Table 1, with the corresponding dimensionless groups given in Table 2.

The numerical technique used here was that developed by Newman [ref. 6]. The nonlinear equations (B) and (D) of Table 1 were linearized by a first order Taylor

series expansion. Then the derivatives were written in second order finite difference form. The boundary at the bromine electrode-membrane interface was taken into account by two methods. In the first method (Equation (E)), the gradient of the potential in the solution phase is equated to the membrane current density. At the electrode entrance, the distributions are calculated using the boundary conditions and Equations (B) through (E). A step is made in the axial direction, and Equations (A) through (E), along with the appropriate boundary conditions are solved using the Crank-Nicholson symmetric form. All the equations are solved implicitly with C_1 - C_6 unknown variables. The iterative technique was carried out until convergence with the Taylor series expansions taken about the solution of the previous iteration.

An alternate method of handling the bromine electrode-membrane interface involved using equation (E') instead of equation (E). The integration was carried out using the trapezoidal method. Since C_4 and C_6 are only needed at the membrane position, these variable were used as dummy variables for storing the summation terms of the integration across the porous electrode. This eliminated extra variables, and allowed the integration to be performed implicitly.

The results of the numerical calculations were checked by comparing the results at the boundary conditions and by verifying intermediate calculations. The step sizes across the porous electrode and along the axial direction were varied to be sure that they did not have a significant effect on the results. The convergence criterion was increased from a relative error of 5 E-6 to 5 E-8. This had no effect on the calculated results.

The calculations using equation (E) took ~7 iterations at the first position and about ~3 iterations at subsequent axial positions for the base case. We devised the second method (use of equation (E')) because it was thought to be more stable since high current-densities and consequently steep gradients were expected with this system. However, the number of iterations to convergence and computational times were about the same. Even when comparing the two methods with high overpotentials, the second method required a few more iterations and slightly more computer time. Therefore, any advantages offered by the second method were not recognized and the method did not appear to justify the added programming complexities which were necessary to implement it.

RESULTS AND DISCUSSION

Model calculations were first done on a base case of parameters which represent reasonable values for a small single cell. The values for these parameters are listed in Table 3. The feed bromide concentration corresponds to approximately a 17% state of charge of an initial solution concentration of 48% HBr. The membrane resistivity was estimated from data for a 24% HBr solution [ref. 3]. The effective solution conductivity was calculated from the conductivity of the electrolyte by [ref. 1].

$$\kappa = \kappa_o \epsilon^{1.5}$$

where $\kappa_o = 0.8\Omega^{-1}cm^{-1}$ [9] and ϵ was estimated by knowing the density of carbon felt [10] and the density of graphite [7]. The dimensionless axial length for the base case was chosen to be Y = 0.0282656. This length corresponds to a cell length to

velocity ratio of 77.5 s (or a 15.5 cm long cell operating with a solution velocity of 0.2 cm/s).

The open circuit potential, OCV, of a prototype SPE hydrogen-bromine cell was measured experimentally. The details of this study were reported elsewhere [ref. 11] and only a summary of the findings will be given here. In figure 2 the mean experimental values of the OCV and the corresponding 95% confidence interval are shown as a function of state of charge. The OCV's for solutions with a charge capacity of 48 wt% HBr (i.e. initial uncharged solution) are lower than the OCV's for a system with a charge capacity of 35 wt%. This indicates that a trade-off exists between the OCV and the charge capacity of the system.

The experimentally measured OCV's of this work were compared to the semi-empirical correlation reported by Yeo and Chin [ref. 3]. Their correlation was derived from experimental data assuming a unit activity of bromine. The correlation predicts somewhat greater open circuit voltages than those found in our experimental work at the lower states of charge. At the highest state of charge, the OCV predicted by the Yeo and Chin correlation was somewhat less than that found experimentally, even though the solubility of bromine in the experimental solution was exceeded (i.e. the bromine activity was unity). The differences could be due to the differences in tribromide and pentabromide concentrations. Overall, though, the comparison between our experimental data and the correlation of Yeo and Chin [ref. 3] was good; See figure 3. Therefore, in this simulation study the correlation of Yeo and Chin [ref. 3] was employed for estimating the OCV of a hydrogen-bromine fuel cell.

Base Case Calculations

Some calculation results for base case conditions are given in figures 4 and 5. The calculations were done for a charging mode of operation with a 200 mV applied polarization. Figure 4 shows the distribution of local current density across the bromine electrode. Under these conditions, only half of the electrode appears to be active. A larger current density occurs near the cell entrance. In figure 5 the distribution of bromide ion across the bromine electrode is shown. At the cell entrance, the bromide concentration is constant as established by the boundary condition. However, a significant concentration variation across the bromine electrode is noted when moving up the cell in the axial direction. Also, one can even note the drop in bromide concentration near the current collector. This, of course, is due to a net consumption of bromide ions. The significance of these calculations will become clear when variations on the base case are discussed.

Bromide Ion Mass Transport

The mass transfer coefficient associated with the bromine electrode for the base case was calculated from the Bird correlation (12) using a velocity of 1 cm/s, and assuming a cylindrical geometry for the fibers of the porous carbon electrode. The calculations show that there is very little effect on cell performance if the magnitude of the product ak_m is lowered by one order of magnitude or increased by two orders of magnitude. Mass transfer of the bromide species to the carbon fibers does not appear to be a problem in this system.

Kinetic Effects

The model calculations are useful for assessing the effectiveness of electrode catalyst. For the base case solution composition , the exchange current density was estimated [ref. 13] using data given by Mastragastino and Gramellini [ref. 14] for a smooth vitreous carbon electrode. As shown in figure 6 , an increase in the exchange current density will only have nominal impact on cell performance. For the hydrogen electrode, the base case exchange current density was estimated by assuming that the ratio of true platinum area to membrane area is 300:1 (i.e. an exchange current density of 0.3 A/cm^2). As shown in figure 7, a further increase in platinum loading or enhancement of surface area will not significantly improve cell performance. However, a loss in platinum activity could severely compromise the performance of the cell. This could occur, for example, if bromine species are transported across the membrane so that they adsorb on the platinum and thus poison the active area.

Membrane Effects

The model calculations demonstrate that the membrane transport properties have the most dramatic impact on cell performance. To demonstrate this, charge and discharge polarization curves are shown in figure 8. The performance is enhanced significantly when the membrane resistivity is lowered by an order of magnitude (psi/10). In this figure, a limiting current density is approached when in the charging mode. This effect is caused by a limit in the diffusion rate of protons across the membrane. The diffusion coefficient of protons was calculated by using the Nernst-Einstein relation and membrane conductivity data. If transport is restricted to only migration of protons associated with fixed ions, then a concentration gradient would not exist. However, since there is a significant amount of free acid in the membrane under these conditions [ref. 3], the transport number for proton does not necessarily equal unity. Thus, a concentration gradient can be established. Actually, the transport mechanism is likely to be more complicated since protons are moved by simple diffusion and migration in the free acid and by migration only along the fixed ion sites. Therefore, the effective transport number is probably not constant with current density. These results indicate that further detailed studies of membrane transport under these conditions are necessary.

Another aspect of the membrane effect deals with the local acid concentration in the solution phase adjacent to the membrane being much lower than the inlet acid concentration. This was shown earlier in figure 5. The computer calculations were modified to account for this effect. The result is shown in figure 9 where the membrane current density along the axial direction is reported. Under these conditions, the changing acid concentration is shown to have a large effect on cell performance.

Scale-up Effects

Some scale-up considerations were examined using the model developed here. For example, increasing the length of the cell in the axial direction results in a lower overall cell current. This is shown in figure 9. Another question which often surfaces when designing a cell deals with ascertaining the optimum thickness of a porous electrode. The effect on cell performance of electrode thickness when the electrolyte velocity is maintained constant is shown in figure 10. As can be seen in this figure, under these conditions an electrode thickness greater than ~1.8 mm only provides marginal improvement in cell performance. As the electrode thickness is increased though, a large volumetric flowrate of electrolyte passes through the cell and consequently, the conversion per pass decreases.

On the other hand, if the volumetric flowrate is maintained constant when examining the effect of electrode thickness, the current density decreases as the electrode thickness increases. This is shown in figure 11. In this case, as the electrode thickness increases, the linear velocity decreases which also decreases the convective transport of mass. As a consequence of this, the concentration of bromic acid drop considerably which causes slower kinetics and thus lower current density.

CONCLUDING REMARKS

A mathematical model was formulated for evaluating design and operating parameters of a hydrogen-bromine fuel cell. The model coupled porous electrode theory applied to the bromine electrode with membrane transport and a planar treatment of the hydrogen electrode.

The parametric studies demonstrate that both the bromine and hydrogen electrode specific surface area and kinetic parameters influence cell performance. However, the magnitude of performance enhancement decreases as catalytic and surface area effects increase. Mass transfer does not seem to be a significant limitation in the bromine electrode.

The calculations indicate that the transport properties of the membrane are the most influential factor in controlling cell performance. Further research appears to be necessary to characterize the proton transport mechanisms in the membrane material.

Finally, the model developed here was demonstrated to be a useful tool for studying cell scale-up effects.

LITERATURE CITED

1. Trainham, J. A. and J. Newman, J. Electrochem. Soc., 130, 533 (1977).

2. Hsu, W.Y. and T.D. Gierke, J. Membrane Sci., 13, 307, (1983).

3. Yeo, R. S., and D-T. Chin, J. Electrochem. Soc., 127, 549 (1980).

4. Newman, J. and C. W. Tobias, J. Electrochem. Soc., 109, 1183, (1962).

5. Newman, J. and W. Tiedemann, A.I.Ch.E. J., 21, 25, (1975).

6. John Newman, Electrochemical Systems, (Prentice-Hall Inc., Englewood, Cliffs, NJ) 1973.

7. CRC Handbook of Chemistry and Physics, R. C. Weast, editor, 59th Edition, (Chemical Rubber Company, West Palm Beach, FL), 1975, a.p F62, b.p.F171.

8. Fedkiw, P. S., and R.K. Watts, J. Electrochem. Soc., 131, 701, (1984).

9. Haase, J., Sauermann, P.F. and K.H. Ducker, Zeit. Phys. Chem., 47, 227 (1965).

10. Jalen, V., Morriseau, B., and L. Swette, NASA Contract DEN 3-198, Giner Inc., 1982.

11. Fritts, S.D., M.S. Thesis, The University of Akron, 1986.

12. Bird, R. B., Stewart, W. E., and E. N. Lightfoot, Transport Phenomena, John Wiley and Sons, New York, 1960.

13. White, R.E., Lorimar, S.E. and R. Darby, J. Electrochem. Soc., 130, 1123, (1983).

14. Mastragostino, M. and C. Gramellini, Electrochimica Acta, 30, 373 (1985).

15. Lanzi, O. and R.F. Savinell, J. Applied Electrochem, 14, 425 (1984).

APPENDIX

Justification of the Equipotential Hydrogen Electrode Assumption

An enlarged view of the porous platinum electrode with a current collector is shown in figure A1. The electronic current must be conducted through the platinum layer to the current collector. The closer the current collector contacts are to each other, the lower the voltage drop will be within the electrode. However, many contact points will block the platinum surface and thus will cause higher overpotentials. This trade-off will now be examined.

Assuming an approximate uniform current distribution, a voltage balance gives [ref. 15]

$$\Delta\phi_1' = \frac{I}{LL'} \rho_e \frac{L^2}{8\delta_e}$$

where L' is the width of the electrode section, and δ_e is the thickness of the platinum layer. In this expression, $\Delta\phi_1'$ is the potential drop in the platinum layer over the distance L/2. If f is the fraction of electrode area exposed to the gas phase, then for a symmetrical current collector system

$$A_t f = LL' \quad (A-2)$$

where A_t is the total area of the membrane. The apparent current density can be written as

$$i' = \frac{I}{A_t} = \frac{f\ I}{LL'} \quad (A-3)$$

Therefore, equation (A-1) becomes

$$\Delta\phi_1' = \frac{i'}{f}\frac{\rho_e}{\delta_e}\frac{L^2}{8} \qquad (A\text{-}4)$$

Of course, as f approaches unity, the contact area between the current collector and the platinum electrode diminishes and the contact resistance may become substantial. This effect, however, is negliected in this analysis.

Assuming the platinum layer consists of a close packing of spherical particles, the Bruggeman equation can be used to relate the effective metal phase resistivity, ρ_e, to the resistivity of solid platinum, ρ_e^o:

$$\rho_e = \rho_e^o(1-\epsilon')^{-3/2}$$

In this expression, ϵ' is the void volume fraction between the platinum particles.

A summary of calculations of the potential drop is shown below. These results indicate that the potential drop along the platinum electrode is small. Therefore, the assumption in the model of an equipotential electrode is justified in most instances.

Calculation of $\Delta\phi_1'$ Summary

$\epsilon' = 0.3$ $\quad \rho_e = 1.81 \times 10^{-5}$ ohm-cm (ref. 7b)

$\delta_e = 30$ μm $\quad i' = 1000$ mA/cm^2

f	L, mm	δ_e, μm	$\Delta\phi_1'$, mV
0.2	2	5	0.9
		10	0.45
	5	5	5.65
		10	2.82
0.5	2	5	0.36
		10	0.18
	5	5	2.26
		10	1.13

Table 1. Dimensionless Model and Boundary Conditions.

$$\frac{\partial C_1}{\partial Y} = \frac{\partial^2 C_1}{\partial X^2} - \Omega\,(C_1 - C_2) \tag{A}$$

$$\beta C_f (C_1 - C_2) = C_2 \exp\{\phi - C_3\} - \exp\{C_3 - \phi\} \tag{B}$$

$$\frac{d^2 C_3}{dX^2} = -\gamma C_f (C_1 - C_2) \tag{C}$$

$$-\lambda (C_6 - C_4) = P^{1/2} \exp\{\sigma - C_5\} - C_4 \exp\{C_5 - \sigma\} \tag{D}$$

$$\eta (C_4 - C_6) = \frac{dC_3}{dX} \tag{E}$$

$$C_6 - C_4 = \chi C_f \int_0^1 (C_1 - C_2)\,dX \tag{E'}$$

Boundary conditions:

$$X = 0 \qquad \frac{dC_1}{dX} = 0 \tag{F}$$

$$\frac{dC_3}{dX} = 0 \tag{G}$$

$$X = 1 \qquad C_3 = C_5 + \theta + \psi (C_6 - C_4) \tag{H}$$

$$\frac{dC_1}{dX} = 0 \tag{I}$$

$$Y = 0 \qquad C_1 = 1 \tag{J}$$

Table 2. Definition of Dimensionless Variables and Parameters.

Variables

$$C_1 = \frac{C_{Br-}^{\delta}}{C_{Br-}^{f\ \delta}}, \qquad C_2 = \frac{C_{Br-}^{\prime\ \delta}}{C_{Br-}^{f\ \delta}}, \qquad C_3 = \frac{\alpha F \phi_2}{RT} \qquad C_4 = \frac{C_{H+}^{\beta}}{1\ \text{mol/l}}, \quad C_5 = \frac{\alpha F \phi_2}{RT},$$

$$C_6 = \frac{C_{H+}^{\beta}}{1\ \text{mol/l}}, \qquad X = x/t, \qquad Y = \frac{\epsilon D_{Br-}}{v_y t^2}$$

Parameters

$$\phi = \frac{\alpha \phi_1 F}{RT}, \qquad \theta = \frac{\alpha U F}{RT}, \qquad \sigma = \frac{\alpha \phi_1' F}{RT}, \qquad C_f = \frac{C_{Br-}^{f\ \delta}}{1\ \text{mol/l}},$$

$$\beta = \frac{nFk_m(0.001\ \text{mol/cc})}{i_{o,ref}},$$

$$\gamma = \frac{anF^2\alpha t^2 k_m(0.001\ \text{mol/cc})}{\kappa RT}, \qquad \Omega = \frac{ak_m t^2}{\epsilon D_{Br-}^{\delta}},$$

$$\lambda = \frac{nFD_{H+}^{\beta}(0.001\ \text{mol/cc})}{t_\beta i'_{o,ref}(1-t_+)}, \qquad P = \frac{P_{H_2}^{\alpha}}{1\ \text{atm}},$$

$$\psi = \frac{\alpha nF^2 D_{H+}^{\beta} R_s(0.001\ \text{mol/cc})}{t_\beta RT\ (1-t_+)}, \qquad \chi = \frac{ak_m t t_\beta (1-t_+)}{D_{H+}^{\beta}},$$

$$\eta = \frac{(0.001\ \text{mol/cc})\alpha F^2 n t D_{H+}^{\beta}}{\kappa RT\ (1 - t^+)}$$

Table 3. Base case values used in parametric studies.

$p_{H_2}^{\alpha}$ = 10 atm. $C_{Br^-}^{f,\delta}$ = 7.45 mole/liter t = 0.3175 cm.

t_β = 0.025 cm. [ref. 3] $D_{H^+}^{\beta}$ = 9.49×10^{-7} [ref. 3] $D_{Br^-}^{\delta}$ = 3.87×10^{-5} [ref. 7a]

R_s = 0.255 Ω-cm^2 [ref. 3] κ = 0.74 $\Omega^{-1}cm^{-1}$ [ref.8,9] a = 280 cm^{-1} [ref. 8]

ρ = 1.49 g/cc μ = 1 g/cm-sec k_m = 0.0866 cm/sec,

$i_{o,ref}$ = 39.7 mA/cm^2 $i'_{o,ref}$ = 300 mA/cm^2 U = 0.816 V [ref. 3]

ϕ_1 = 1.016 V ϵ = 0.95 t_+ = 0.975

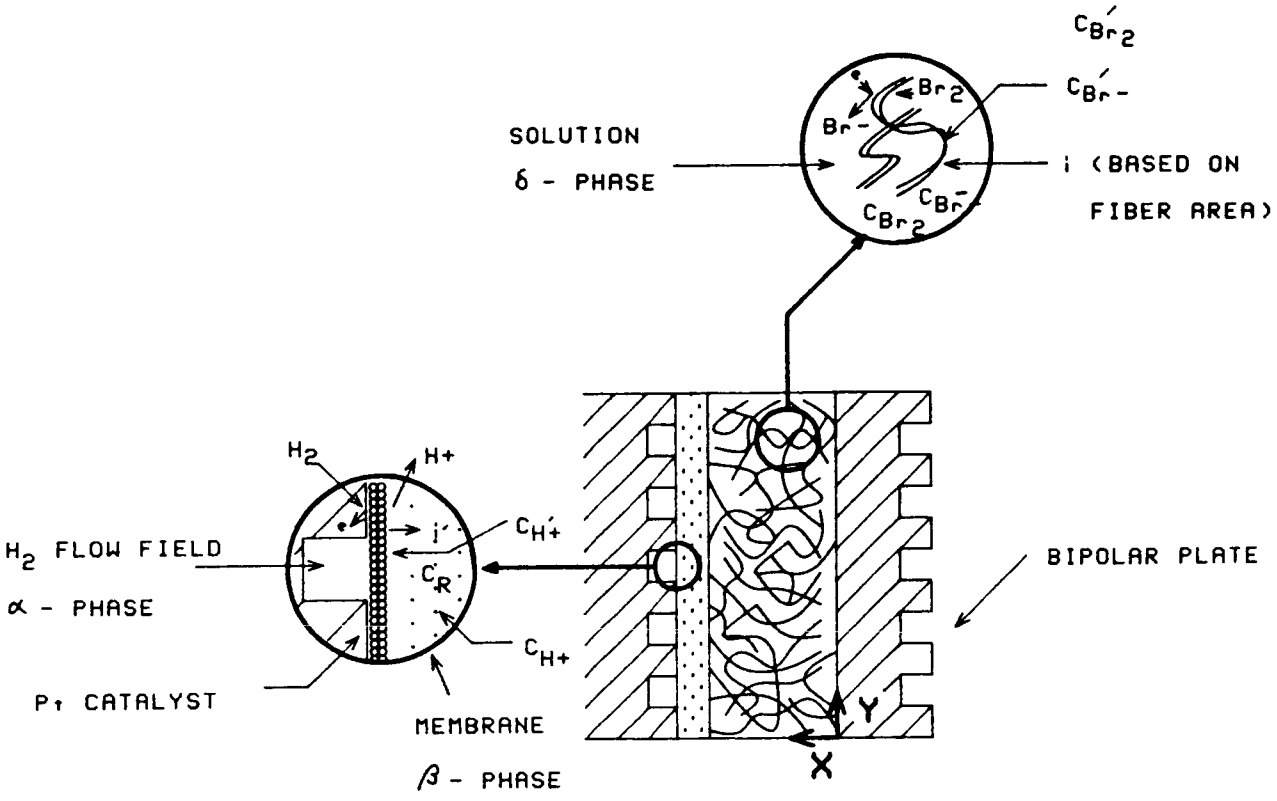

Figure 1: Diagram of H_2-Br_2 fuel cell details for mathematical modeling.

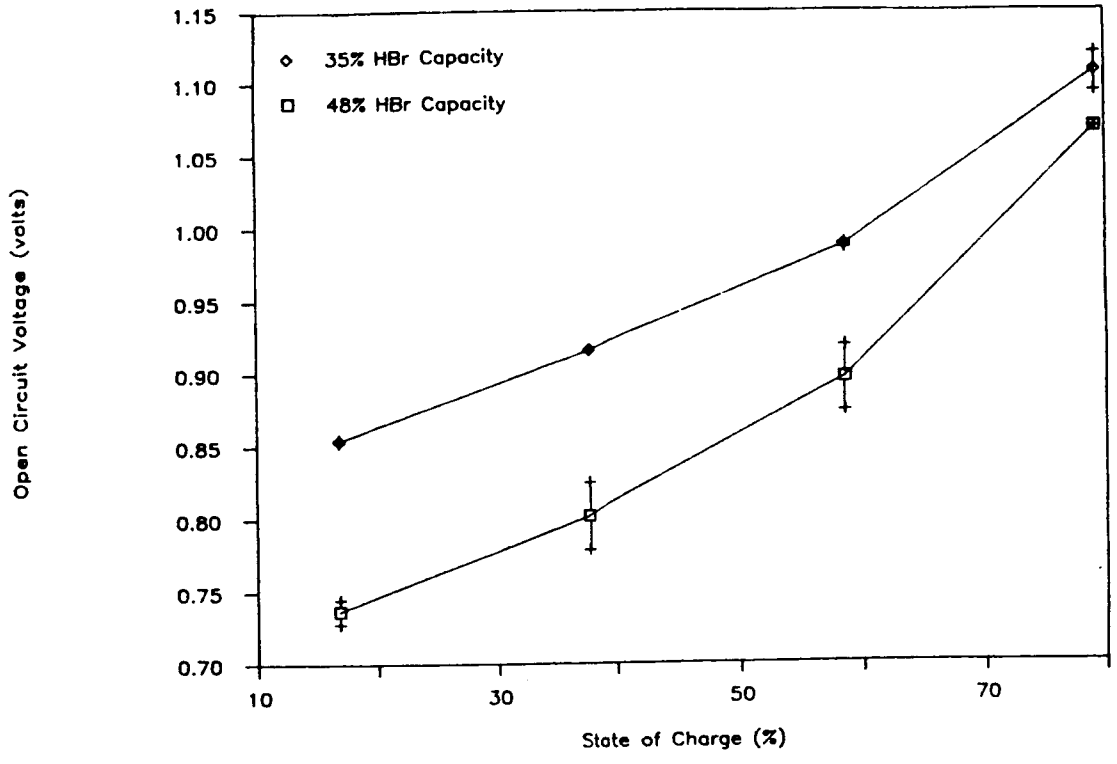

Figure 2: Mean open circuit voltages of H_2-Br_2 cell.

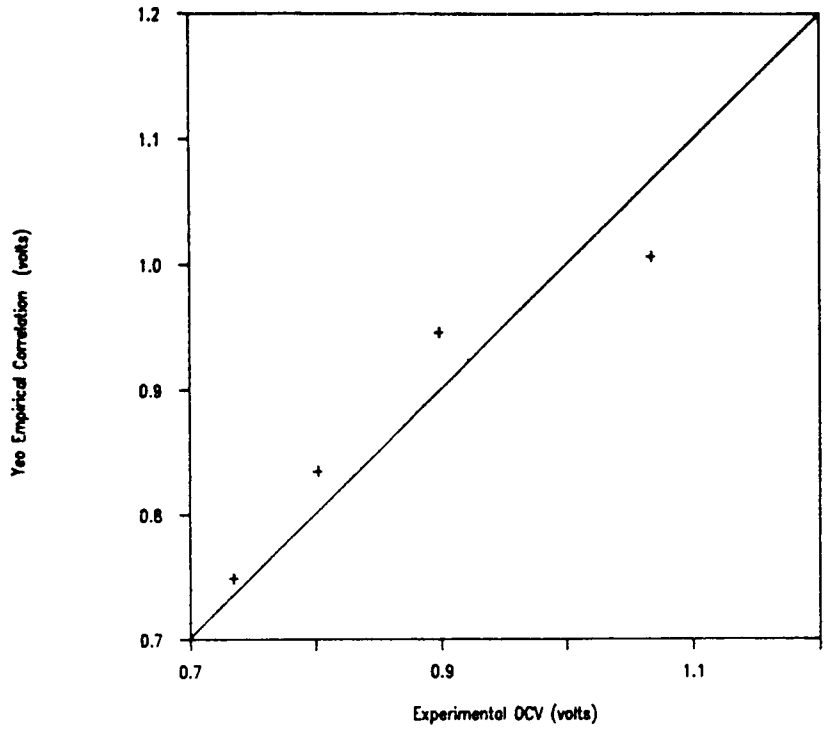

Figure 3: Comparison of experimental open circuit voltages for solutions with 48% HBr charge capacity to open circuit voltages predicted by correlation of Yeo and Chin.

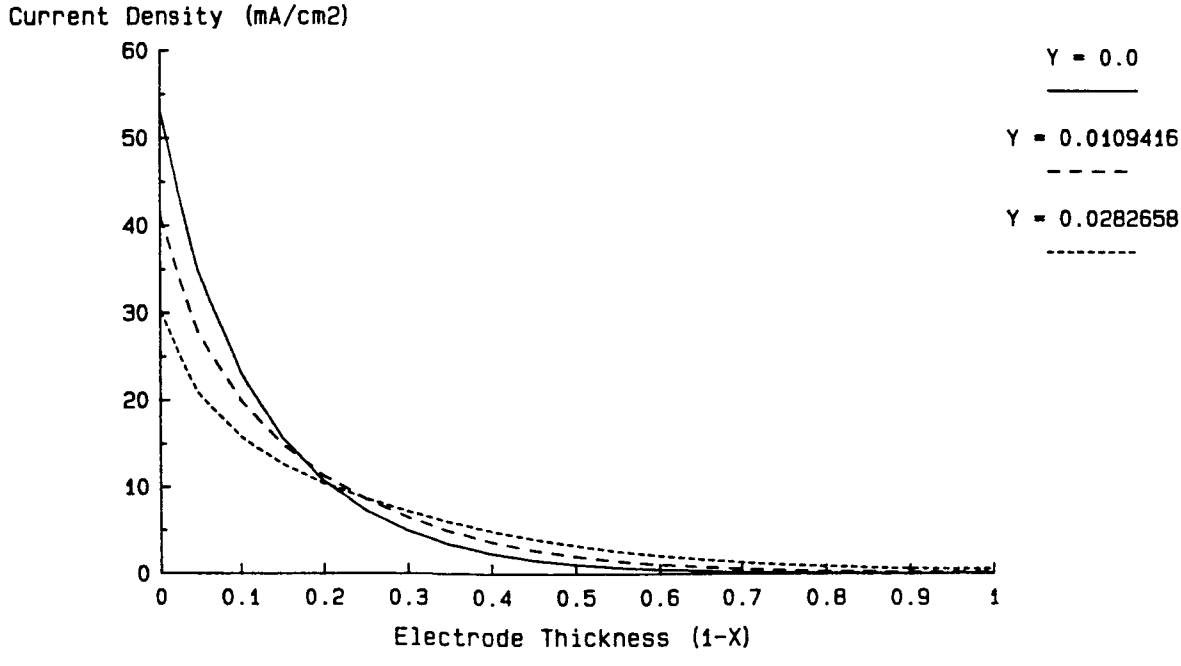

Figure 4: Local current density distribution in porous bromine electrode.

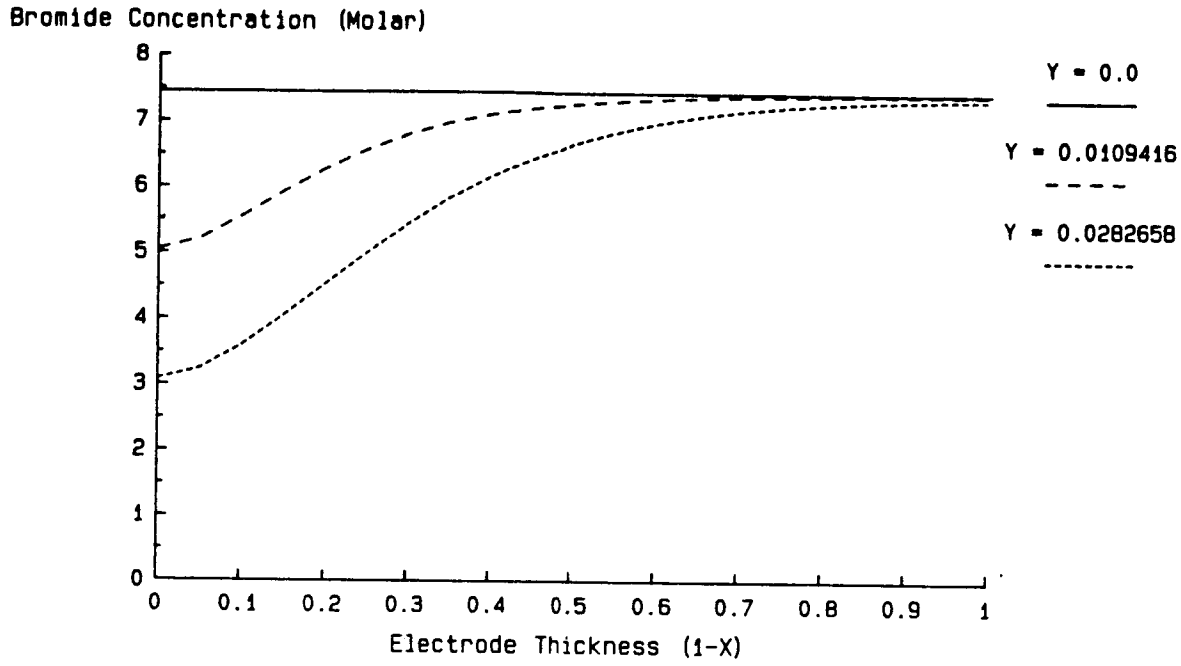

Figure 5: Local bromide ion distribution in porous bromine electrode.

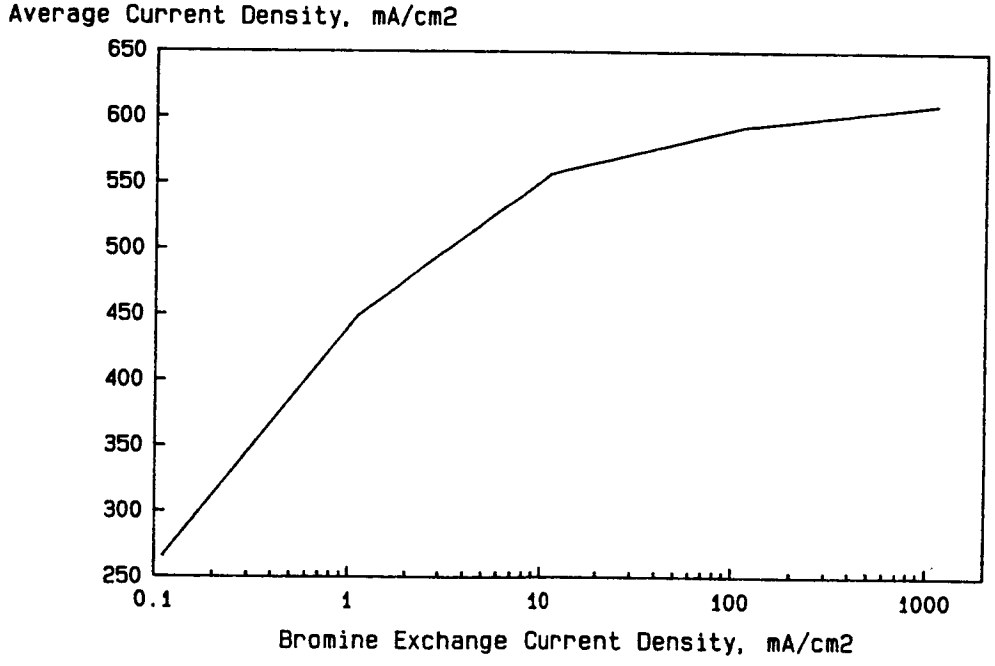

Figure 6: The effect of bromine electrode activity on average cell current density.

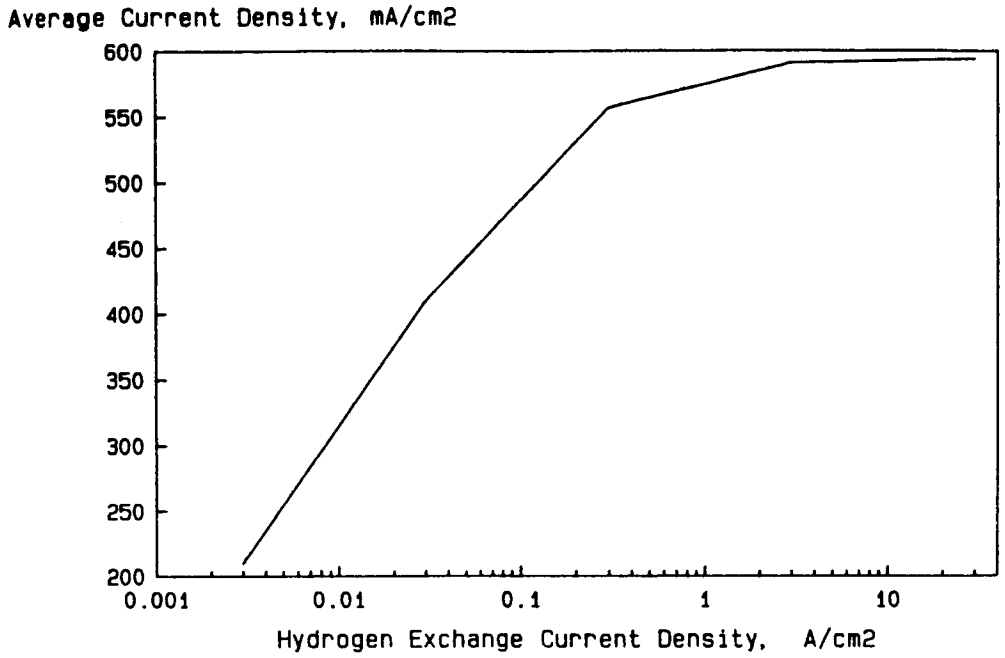

Figure 7: The effect of hydrogen electrode activity on average cell current density.

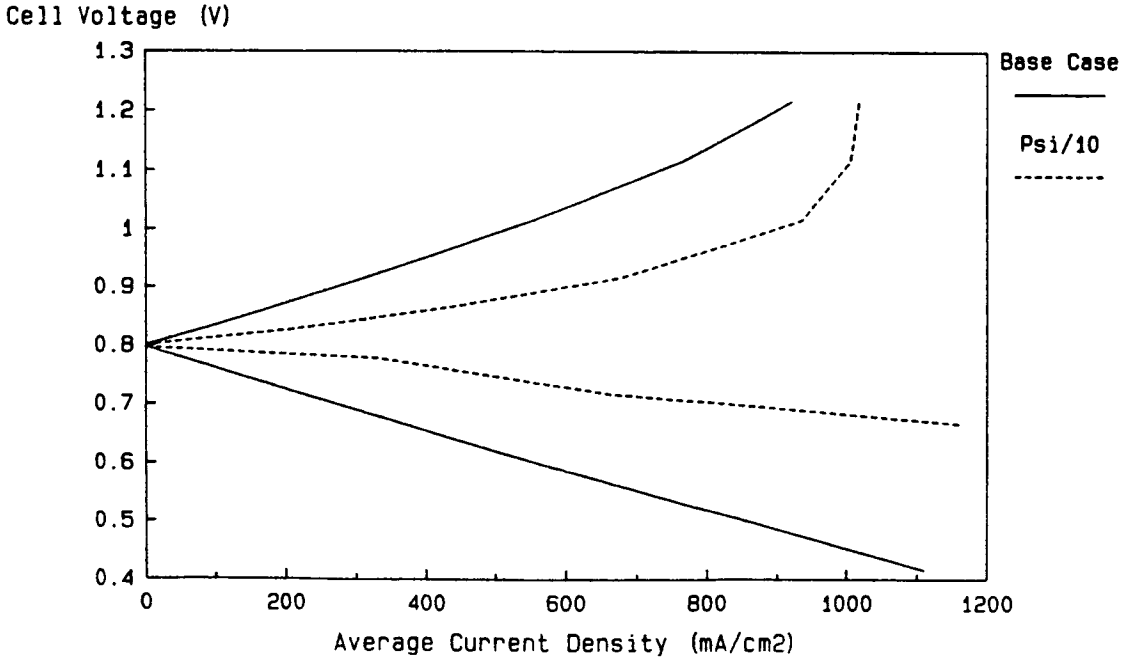

Figure 8: Predicted cell polarization curves.

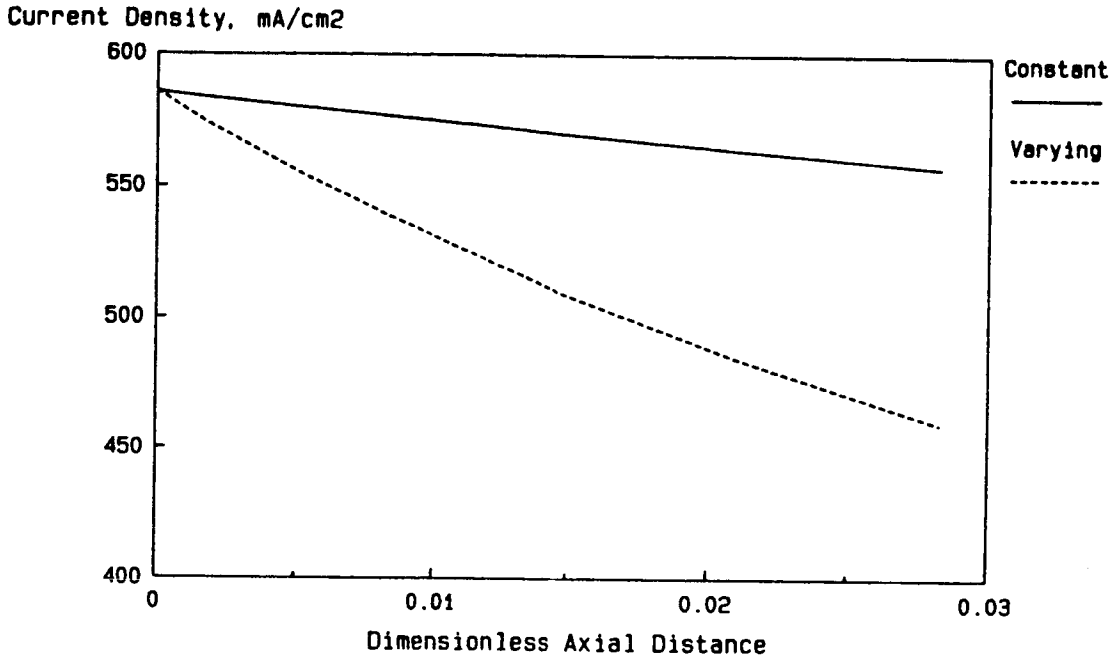

Figure 9: The effect of membrane proton concentration on membrane current density.

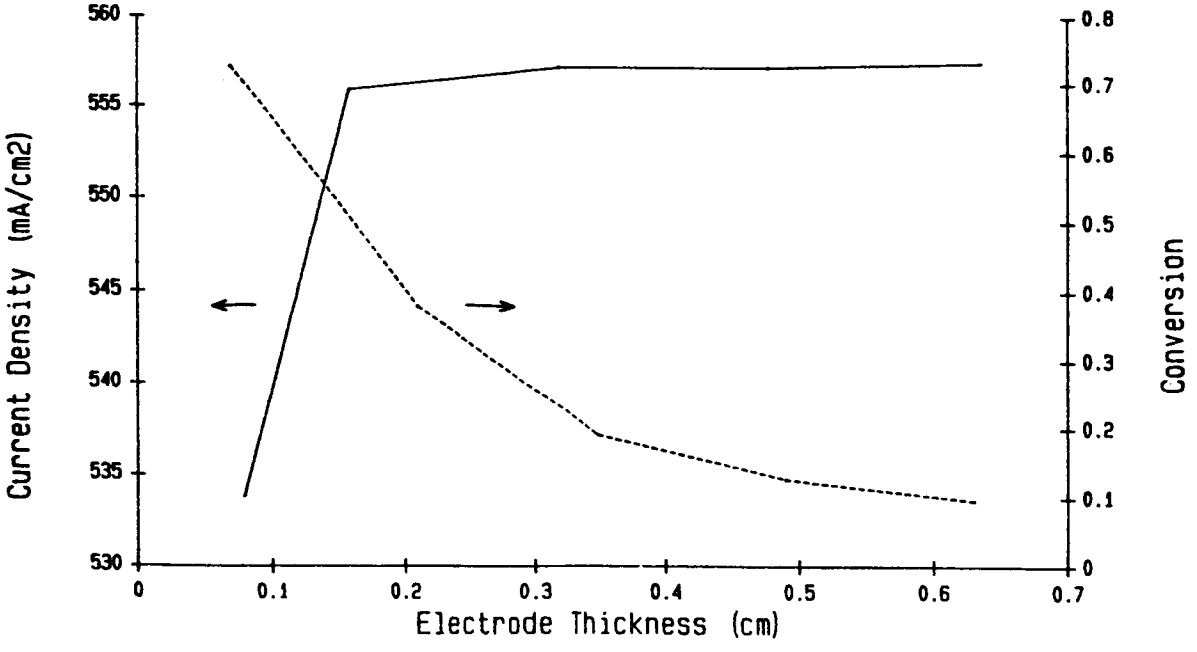

Figure 10: The effect of electrode thickness on cell performance with constant solution velocity.

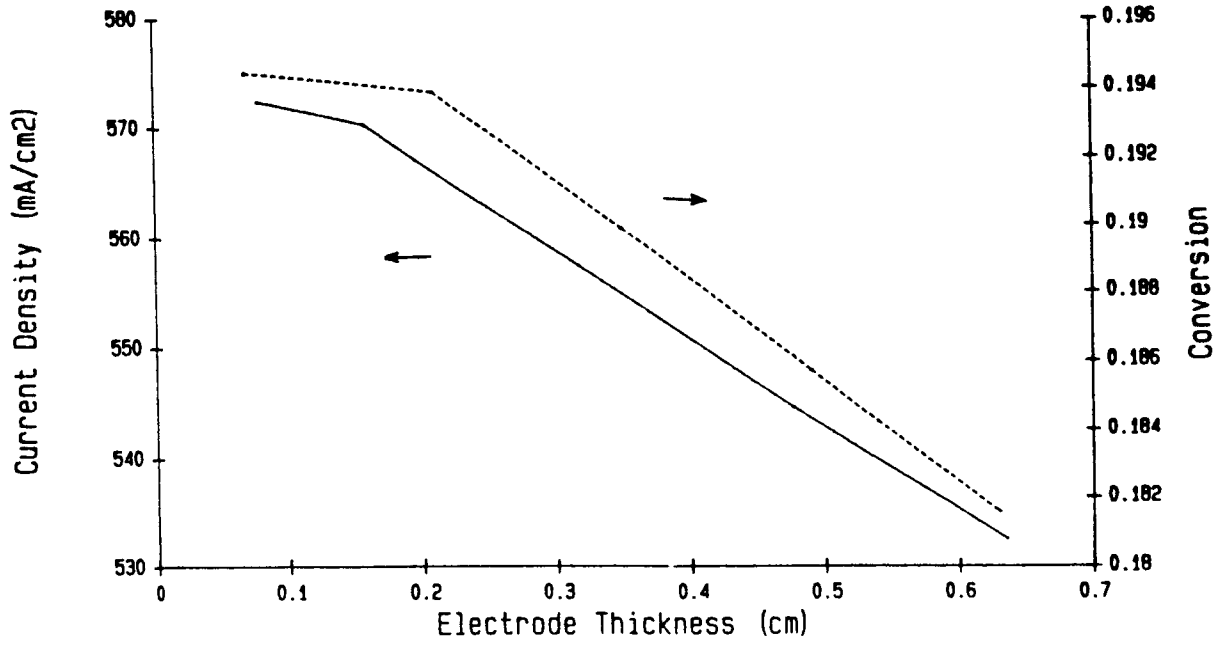

Figure 11: The effect of electrode thickness of cell performance with constant solution volumetric flow rate.

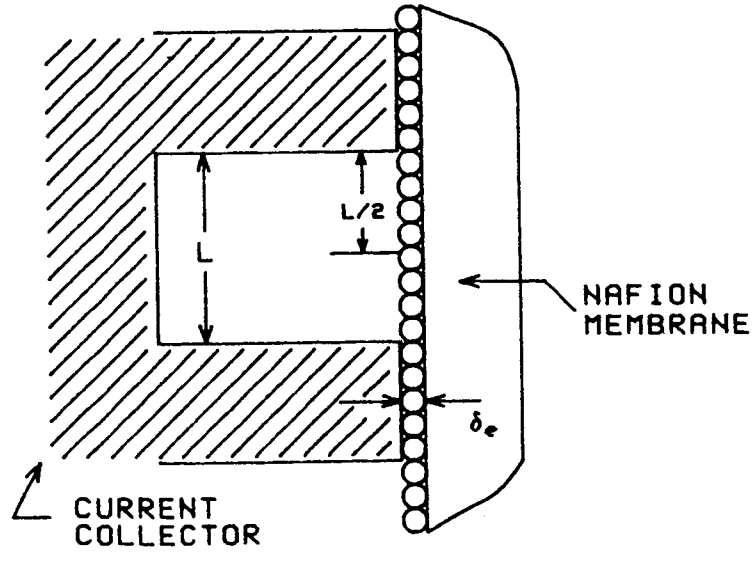

Figure A1: Expanded view with dimensions of a hydrogen electrode of a hydrogen-bromine SPE cell.